electrochem

MDPI

Article

Understanding the Effect of Zn Doping on Stability of Cobalt-Free P2-$Na_{0.60}Fe_{0.5}Mn_{0.5}O_2$ Cathode for Sodium Ion Batteries

Devendrasinh Darbar [1], M. V. Reddy [2,*] and Indranil Bhattacharya [1,*]

[1] Department of Electrical and Computer Engineering, Tennessee Technological University, Cookeville, TN 38505, USA; dudarbar42@tntech.edu
[2] Centre of Excellence in Transportation Electrification and Energy Storage (CETEES), Hydro-Québec, 1806, Lionel-Boulet Blvd., Varennes, QC J3X 1S1, Canada
* Correspondence: reddymvvr@gmail.com (M.V.R.); ibhattacharya@tntech.edu (I.B.)

Abstract: In this work, we report a sol-gel synthesis-based Zn-doped $Na_{0.6}Fe_{0.5}Mn_{0.5}O_2$ (NFM) cathode and understand the effect of Zn doping on the crystal structure and electrochemical performances such as discharge capacity and rate capability. Detailed X-Ray diffraction (XRD) pattern analysis indicated a decrease in the Na-layer thickness with Zn doping. Small amount of Zn^{2+} dopant (i.e., 2 at.%) slightly improved cycling stability, reversibility, and rate performances at higher discharge current rates. For example, at 1 C-rate (1 C = 260 mAh/g), the Zn^{2+}-doped cathode retained a stable reversible capacity of 72 mAh/g, which was ~16% greater than that of NFM (62 mAh/g) and showed a minor improvement in the capacity retention of 60% compared to 55% for the pristine NFM after 65 cycles. Slight improvement in the electrochemical performance for the Zn-doped cathode can be attributed to a better structural stability, which prevented the initial phase transition and showed the presence of electrochemical active $Fe^{3+/4+}$ even after 10 cycles compared to NFM.

Keywords: P2-type cathode; cobalt-free; Zn doping; sol-gel process; structural analysis; sodium-ion battery

Citation: Darbar, D.; Reddy, M.V.; Bhattacharya, I. Understanding the Effect of Zn Doping on Stability of Cobalt-Free P2-$Na_{0.60}Fe_{0.5}Mn_{0.5}O_2$ Cathode for Sodium Ion Batteries. *Electrochem* **2021**, *2*, 323–334. https://doi.org/10.3390/electrochem2020023

Academic Editor: Masato Sone

Received: 16 April 2021
Accepted: 24 May 2021
Published: 2 June 2021

1. Introduction

Sodium-ion battery technology is considered as one of the potential alternatives to existing lithium-ion batteries. Sodium metal is abundant, and has lower desolvation and activation energies than lithium. Among sodium host intercalation materials, layered sodium transition metal oxide materials are considered as excellent choices for sodium-ion batteries [1]. Sodium layered oxides (Na_xTMO_2) are composed of duplicate sheets of TMO_2 (TM:Fe, Mn, Co [2–4]) where Na ions are intercalated between the oxide layers. O3 phase occurs when $0.7 \leq x \leq 1$ [5–7], P2 when $x \approx 0.7$ [1,6,8–11] and P3 when $x \approx 0.5$ [12], where x indicates the amount of sodium present in the cathode. P2-type cathodes show better reversible capacity due to lower phase transition and less misalignment of Na-ions than O3 types [6,13,14]. P2-type phase mainly occurs when x ~ 0.7, stacking of the oxide layers are in ABBA fashion and Na ions are shared either entirely as edge-shared or face-shared as shown in (Figure 1).

P2-type cathodes such as $Na_{0.66}Fe_{0.5}Mn_{0.5}O_2$ [6,9,10], $Na_{0.67}Fe_{0.33}Mn_{0.67}O_2$ [15], $Na_{0.67}Mn_{0.8}Fe_{0.1}Ti_{0.1}O_2$ [11], $Na_{0.67}Co_{0.67}Mn_{0.33}O_2$ [16], $Na_{0.67}Ni_{0.33}Ti_{0.67}O_2$ [17] have been extensively studied. Among all, $Na_xFe_{0.5}Mn_{0.5}O_2$ (NFMO) is an intriguing cathode material and shown promising high specific capacity of 190mAh/g, on a par with mainstream Li-ion battery cathodes ($LiNi_{0.8}Mn_{0.1}Co_{0.1}O_2$ [18]). Though NFMO cathode is highly attractive, because of redox active Mn^{3+} and Fe^{3+} ions, the cathode material undergoes degradation f due to the irreversible phase transformations at higher voltages [6]. Yabuuchi et al. [6], reported a phase transition from P2 to OP4 when charged to 4.2 V because of the

Jahn Teller distortion cause from Fe^{4+} ion. Talaie et al. [19] argued that the electrochemical degradation of NFMO owed to the migration of transition metal ions into the Na layer.

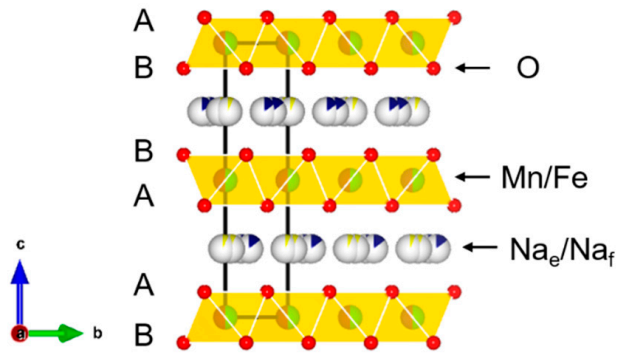

Figure 1. Crystal structure of P2-type $Na_{0.67}Fe_{0.5}Mn_{0.5}O_2$ cathode with a typical hexagonal layered lattice of space group P63/mmc symmetry, having Na occupancy with Na_e (edge share) and Na_f (face share) amalgamated with yellow and navy-blue colors, respectively. Oxygen atoms are represented in red, Mn atom in orange and Fe atom in black.

Electrochemical performances of NFMO can be improved by stabilizing the phase transitions, promoting higher Na-ion diffusion by increasing the d-spacing between interlayers and better electronic conductivity. Doping the cathodes material is an effective technique to enhance the cycling stability of P2-type sodium ion batteries [8,19–22]. Al-doped NFMO increases the d-spacing which enhances the Na^+ diffusion, mitigates the irreversible phase transition and improve structural stability and rate performances [20]. Ti doping at Fe or Mn sites in NFMO improved the rate performances and cycling stability by increasing the Na-layer in the crystal structure [8,23].

Zn^{2+} dopant is known to improve the O3-$NaNi_{0.2}Fe_{0.35}Mn_{0.45}O_2$, $Na_3Ni_2BiO_6$, $Na_3Ni_2SbO_6$ by suppressing the phase transition, stabilize the crystal structure and alleviate the voltage fading [24–26]. Wang et al. [27] showed Zn^{2+} was doped nonuniformly in P2-$Na_{0.67}Ni_{0.33}Mn_{0.67}O_2$ by minimizing the Ni content and that it improved cycling stability by mitigating the particle cracking, but showed low initial specific capacity of ~120 mAh/g at 0.1 C cycled at 4.5 V. Xu et al. [28] reported P2-type $Na_{0.67}Mn_{0.6}Fe_{0.4\text{-}x\text{-}y}Zn_xNi_yO_2$ cathode synthesized via acetate decomposition where Zn^{2+} and Ni^{2+} was doped at Fe^{3+} site. It shows better capacity retention and higher average discharge voltage by effectively alleviate the Jahn–Teller (JT) distortion from Mn^{3+} but did not clearly explained the phenomenon of minimizing the JT distortion. Wu et al. [29] has shown a detailed understanding of Zn^{2+}-doped P2-$Na_{0.66}Ni_{0.33}Mn_{0.67}O_2$ at Ni sites. Zn^{2+} helps to reduce the distortion degree of Ni-O octahedron in the Na-Ni-Mn-O structure and it also improves the reversibility of P2-O2 phase transition.

In this work, we report a wet-solution-based Zn^{2+} doping on $Na_{0.60}Fe_{0.5}Mn_{0.5}O_2$ (NFM) cathode material has varied contents of Zn^{2+} ion from 1–10 at.%. We investigated detailed material crystallographic structures, understanding the effect of Zn^{2+} in NFM cathode on its electrochemical performances. Rietveld refinement technique was performed on the X-Ray Diffraction (XRD) patterns to calculate the thicknesses of transition metal and Na-layers for undoped and Zn-doped NFM samples. We aimed to solve the fading discharge capacity of NFM by improving the structural stability and prevent the phase transition. We have attempted to reduce the Na content to 0.60 and expect an increase in the *c*- lattice parameter from the strong repulsion of O_2^{-}-$^{-}$ between the adjacent transition metal oxide layers in the structure and by incorporating higher ionic radius Zn^{2+} (0.74 Å) ion in the crystal structure. Overall, the findings reported here highlight slight improvements in the cycling stability, reversibility, and rate performance.

2. Materials and Methods

2.1. Material Synthesis

P2 type—$Na_{0.60}Fe_{0.5}Mn_{0.5-x}Zn_xO_2$ (x = 0, 0.01, 0.02, 0.05, 0.10) was synthesized via sol gel technique. The appropriate amount of precursor CH_3COONa (10% excess, Sigma Aldrich, St. Louis, MO, USA), $Fe(NO_3)_3.9H_2O$ (Alfa Aesar, Haverhill, MA, USA), $(CH_3COO)_2Mn.4H_2O$ (Sigma Aldrich) and $(CH_3COO)_2Zn.2H_2O$ (Alfa Aesar) (0.60:0.5:0.5:0 molar ratio for x = 0, 0.60:0.5:0.0.49:0.01 molar ratio for x = 0.01, 0.60:0.5:0.48:0.02 molar ratio for x = 0.02, 0.60:0.5:0.45:0.05 molar ratio for x = 0.05, 0.60:0.5:0.40:0.10 molar ratio for x = 0.10) and citric acid (Alfa Aesar) were dissolved in deionized water. The mixed solution was heated at 80 °C and stirred until distilled water evaporated. The dried powder was ground and underwent first-phase heating at 400 °C (heating rate, 5 °C/min) for 4 h to decompose all acetate and nitrate, followed by second-phase heating at 875 °C (heating rate—5 °C/min) for 15 h in air to procure the final P2-type structure cathode material. The final calcined powder sample was stored in an Argon-filled glove box (H_2O, $O_2 \leq 0.1$ ppm) to avoid the exposure to air. The notation for the $Na_{0.60}Fe_{0.5}Mn_{0.5-x}Zn_xO_2$ (x = 0, 0.01, 0.02, 0.05, 0.10) assigned as Zn-0 or NFM, Zn-1, Zn-2, Zn-5, and Zn-10 respectively

2.2. Material Characterization

X-ray diffraction (XRD) was performed using Rigaku Ultima IV diffractometer with a D/tex ultra-high-speed detector over the 2θ range from 10° to 80° at a scan speed of 2°/min with Cu Kα radiation (power setting 40 kV, 44 mA). Rietveld refinements on the XRD pattern were performed using Rigaku software. The initial structural model of $Na_{0.67}Fe_{0.5}Mn_{0.5}O_2$ was adopted from the Inorganic Structural Database [30]. For Rietveld refinement, parameters such as oxygen positional parameter, lattice constant and sodium occupancy were refined. The total amount of sodium content was constrained to the nominal chemical composition i.e., 0.60, occupancy of Fe, Mn, Zn and the atomic coordinates were constrained accordingly to the sample composition. The morphology of the powder was observed using a Quanta 200 Environmental scanning electron microscope (SEM).

2.3. Electrochemical Characterization

The electrochemical characterization was analyzed by fabricating the cathode in the coin cell CR2032 (20.0 mm(diameter) × 3.2 mm(height), United Minerals and Chemical Corporation) using Na metal as the counter electrode, two glass microfibers (Whatman DBS 30) as the separator and a slurry cast cathode as the working electrode. Cathodes were prepared by casting the active material slurry on a carbon-coated aluminum current collector. Slurries were prepared by mixing the active material, a conducting agent (Super P, TIMCAL) and binder (Kynar PVDF) with the mass ratio 80:10:10 respectively and N-Methyl-2-Pyrrolidone (NMP) was used as a solvent. The cathode was dried under vacuum at 90 °C overnight. The active material weight on the circular disc electrode was approximately ~2–3 $mg \cdot cm^{-2}$. The electrolyte was 1.0 M solution of NaClO4 and 2% fluoroethylene carbonate (FEC) was used as an additive in propylene carbonate. All the coin cells were assembled in an Argon filled glovebox (H_2O, $O_2 \leq 0.1$ ppm). Galvanostatic cycling on the assembled coin cell was evaluated using MACCOR Series 4000 battery tester at various current rate from 0.05 C to 4 C (1 C = 260 mAh/g) cycled between 1.5–4.2 V and 1.5–4.0 V vs. Na^+/Na. Cyclic voltammetry (CV) measurements were performed using Biologic SP-200 at a scan rate of 0.1 mV/s cycled between 1.5–4.2 V vs. Na^+/Na.

3. Results and Discussion

3.1. Structural and Morphological Studies of Undoped and Zn-Doped $Na_{0.60}Fe_{0.5}Mn_{0.5-x}Zn_xO_2$ (NFM) Cathodes

Crystallographic evaluations of P2-type $Na_{0.60}Fe_{0.5}Mn_{0.5-x}Zn_xO_2$ (x = 0, 0.01, 0.02, 0.05, 0.10) cathode powder was performed using the X-ray Diffraction patterns shown in Figure 2. All the powder samples represented P2-type structure with a typical hexagonal layered lattice having a space group P63/mmc symmetry, which is isostructural to P2-type

$NaCoO_2$ [31]. Samples with Zn-2, Zn-5 and Zn-10 detect impurity formations of $ZnFe_2O_4$ (DB card number 00-002-1030) as shown in Figure 2b. No impurities were observed for Zn-0 and Zn-1.

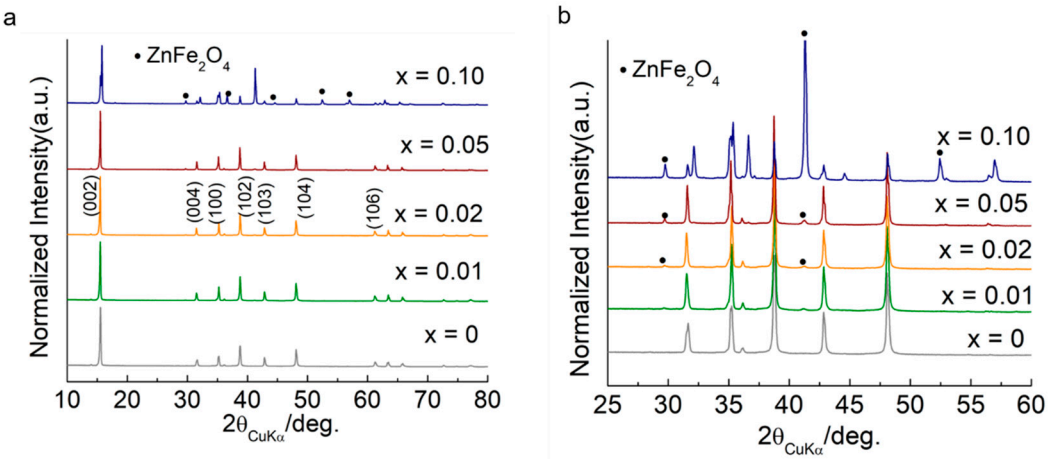

Figure 2. X-ray diffraction (XRD) patterns for P2-$Na_{0.60}Fe_{0.5}Mn_{0.5-x}Zn_xO_2$ (x = 0, 0.01, 0.02, 0.05, 0.10) cathodes powder in the 2θ range (**a**) 10–80° (**b**) 25–60°, expanded view to observe the impurities formation from Zn-2 cathodes onwards. The impurities are marked with (•) representing $ZnFe_2O_4$.

Morphological assessment for undoped/doped NFM cathodes were performed using SEM images. All the synthesized samples showed distinct shape particles having an average particle size in range of ~0.5–2.5 µm, except for Zn-10 sample as shown in Figure 3. (The particle sizes were calculated with the help of Image J Software on SEM image). With incorporation of Zn^{2+} dopant up to 2 at.%, no major morphological changes were observed compared to the undoped NFM. For the Zn-5 sample, smaller lumped sized particles were observed, and Zn-10 showed a larger amount of minute chunks of particles covering the bigger particles, which are marked with circle/ellipse in Figure 3d,e. These lumped particles might be corresponding to $ZnFe_2O_4$ impurities on the hexagonal NFM particles.

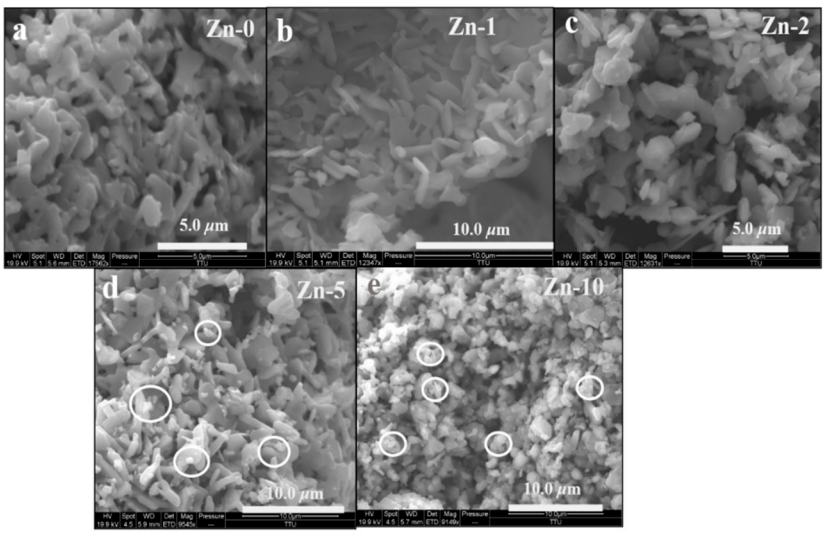

Figure 3. (**a**–**e**) Scanning electron micrograph images of $Na_{0.60}Fe_{0.5}Mn_{0.5-x}Zn_xO_2$ (x = 0, 0.01, 0.02, 0.05, 0.10). Circle/ellipse mark on SEM image (**d**) Zn-5 and (**e**) Zn-10 shows the secondary particle.

Rietveld refinements were performed on XRD patterns for samples Zn-0, Zn-1 and Zn-2 cathode powder respectively using Rigaku software as shown in Figure 4a–c. This helps to determine atomic coordinates, refined lattice parameters and metal occupancy

(Tables S1–S3) in cathode composite. The above parameters will be required to calculate the thickness of the Na-layer and transition metal layer for the cathode sample by substituting the oxygen coordinate value in Equations (1) and (2) mentioned below. The parameters taken into consideration during refinement mentioned earlier in Section 2.2. Refined lattice parameters and calculated Na-layer/transition metal layer thicknesses are given in Table 1. The expected oxidation states present in P2-type $Na_{0.67}Fe_{0.5}Mn_{0.5}O_2$ for Fe is +3 (Fe^{3+} ionic radius ~0.64 Å) and for Mn is Mn^{3+}(0.64 Å) and Mn^{4+}(0.53 Å) ions [6,8,20]. It is expected that by doping the Zn^{2+} (0.74 Å, [32]) in NFM cathode, 'c' lattice parameter will increase (Figure 4d).

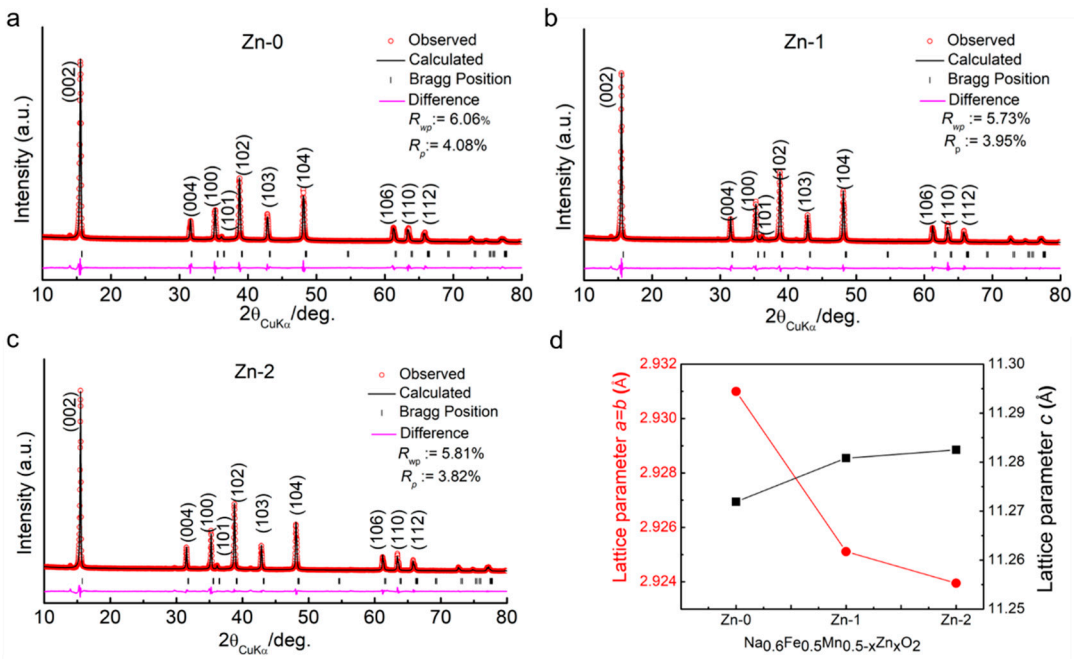

Figure 4. Rietveld refinement was performed on the XRD pattern of P2-type $Na_{0.60}Fe_{0.5}Mn_{0.5-x}Zn_xO_2$ (**a**) x = 0 (Zn-0) (**b**) 0.01 (Zn-1) and (**c**) 0.02 (Zn-2) cathode powder using Rigaku software. Observed data is represented as red circles, calculated Rietveld data model as a black line, the difference between the data and model is shown with magenta color and Bragg position is shown using a vertical reflection marker. All Rietveld fit data has R_{wp} and R_p values below 10%. (**d**) Graphical representation of the lattice parameter *a* and *c* observed after Rietveld refinement on the XRD pattern of Zn-0, Zn-1 and Zn-2 cathodes sample.

Table 1. Crystallographic refined lattice parameters and calculated TMO_2 /Na-layer thickness value for Zn-0, Zn-1 and Zn-2 cathodes.

Sample	a (Å)	c (Å)	R_{wp} (%)	R_p (%)	$d_{(002)}$ (Å)	Oxygen Coordinate (z_{ox})	T_MO_2 (Å)	Na-Layer (Å)
Zn-0	2.93	11.27	6.06	4.08	5.63	0.0934	2.11	3.52
Zn-1	2.92	11.28	5.73	3.95	5.64	0.0975	2.20	3.44
Zn-2	2.92	11.28	5.81	3.82	5.64	0.0993	2.24	3.39

The transition metal and Na layer thicknesses can be calculated from Equations (1) and (2) as mentioned below. Similar studies were performed by Li et al. [33].

$$d_{(002)} = d_{(slab)} + d_{(interslab)} \quad (1)$$

$$d_{(slab)} = 2\, d_{(002)} - (1 - 2z_{ox}) \times c \quad (2)$$

Here $d_{(002)}$ denotes the d-spacing determined from (002) peak, $d_{(slab)}$ denotes the transition metal layer (TMO_2) thickness and $d_{(interslab)}$ denotes the Na-layer thickness, z_{ox}

is the coordinate of oxygen in the crystal structure obtained after Rietveld refinement (See Tables S1–S3) and *c* is the refined lattice parameter of the cathode sample. The results are summarized in Figure 5 (shows the schematic of crystal structure plotted in Vesta software [34]) and Table 1. Calculated Na-layer thickness for Zn-1 was 3.44 Å and for Zn-2 was 3.39 Å which decreased by ~2.5–4% compared to Zn-0. Decrease in the Na-layer thickness for Zn-2 results from the increase in its transition metal thickness layer. The increased thickness of TMO_2 slab may be attributed to the low bond dissociation energy of Zn-O (ΔHf^{298K} = 284.1 kJ/mol) compared to Fe-O (ΔHf^{298K} = 409 kJ/mol) and Mn-O (ΔHf^{298K} = 402 kJ/mol) [35]. Based on this work, we-doped Ti^{4+} in our future work, where Ti-O has higher bond dissociation energies (ΔHf^{298K} = 662 kJ/mol) [23].

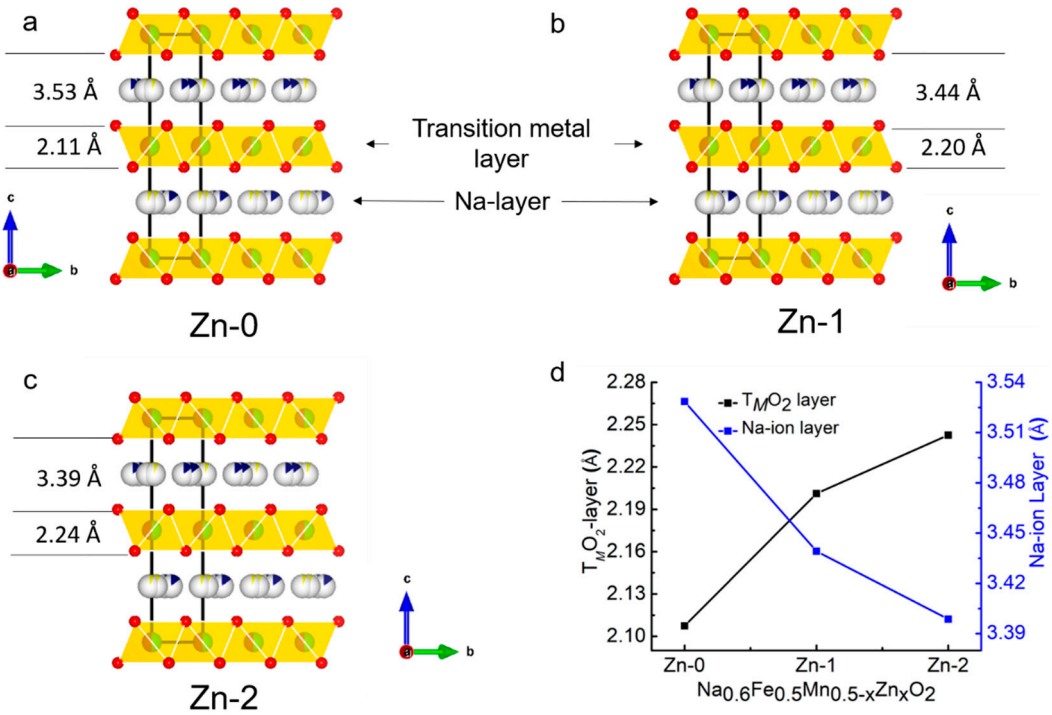

Figure 5. Schematic of layered crystal structure of (**a**) Zn-0 (**b**) Zn-1 and (**c**) Zn-2 cathode showing Na- and TMO_2-layer thickness value. (**d**) Represents the relationship of TMO_2 slab and Na-layer thickness for Zn-0, Zn-1 and Zn-2 cathode respectively.

3.2. Electrochemical Studies for Doped and Undoped NFM

Evaluation of electrochemical performances for Zn-0, Zn-1 and Zn-2 cathode were investigated by understanding the cycling stability, rate performances and voltage profile curves for cathode sample obtained from the assembled coin cell CR2032 (detailed fabrication of the coin cell is mentioned in Section 2.3). Figure 6a shows the galvanostatic cycling performance of pristine NFM and Zn-doped NFM cathode cycled between 1.5–4.2 V vs. Na/Na^+ at 0.05 C (1 C = 260 mAh/g). Zn-0, Zn-1, and Zn-2 indicate an initial discharge capacity of ~193, ~188, and ~175 mAh/g which was reduced to ~107, ~99 and ~104 mAh/g after 65 cycles shows a capacity retention of ~55%, ~52% and ~60% respectively. The difference in initial discharge capacities among the undoped/doped NFM was because Zn^{2+} was doped at Mn^{3+} sites and it is an electrochemically inactive within the corresponding voltage window (detailed explanation for low initial specific capacity for Zn-2 cathode is mentioned below). Figure 6b shows the normalized capacity vs. cycle number to distinguish the capacity degradation of different cathode composite with every cycle and Zn-2 cathode sample represents better cycling stability. Figure 6c shows rate performances of NFM and Zn-doped NFM cycled between 1.5–4.2 V vs. Na/Na^+ at different C rates. At 1 C-rate, Zn-2 cathode shows a stable reversible capacity of 72 mAh/g which was ~16% higher than that of Zn-0 (62 mAh/g). Zn-0 shows an initial discharge

capacity of ~190 mAh/g at 0.05 C and cycled back to 0.05 C after 4 C, and has a discharge capacity of ~143 mAh/g, which indicates a loss of ~26% capacity, whereas Zn-2 showed a capacity loss of ~17%. This slightly improved electrochemical performance for Zn-2 sample might be because no initial phase transition occurs at higher voltage which helps to stabilize the crystal structure initially (explained later).

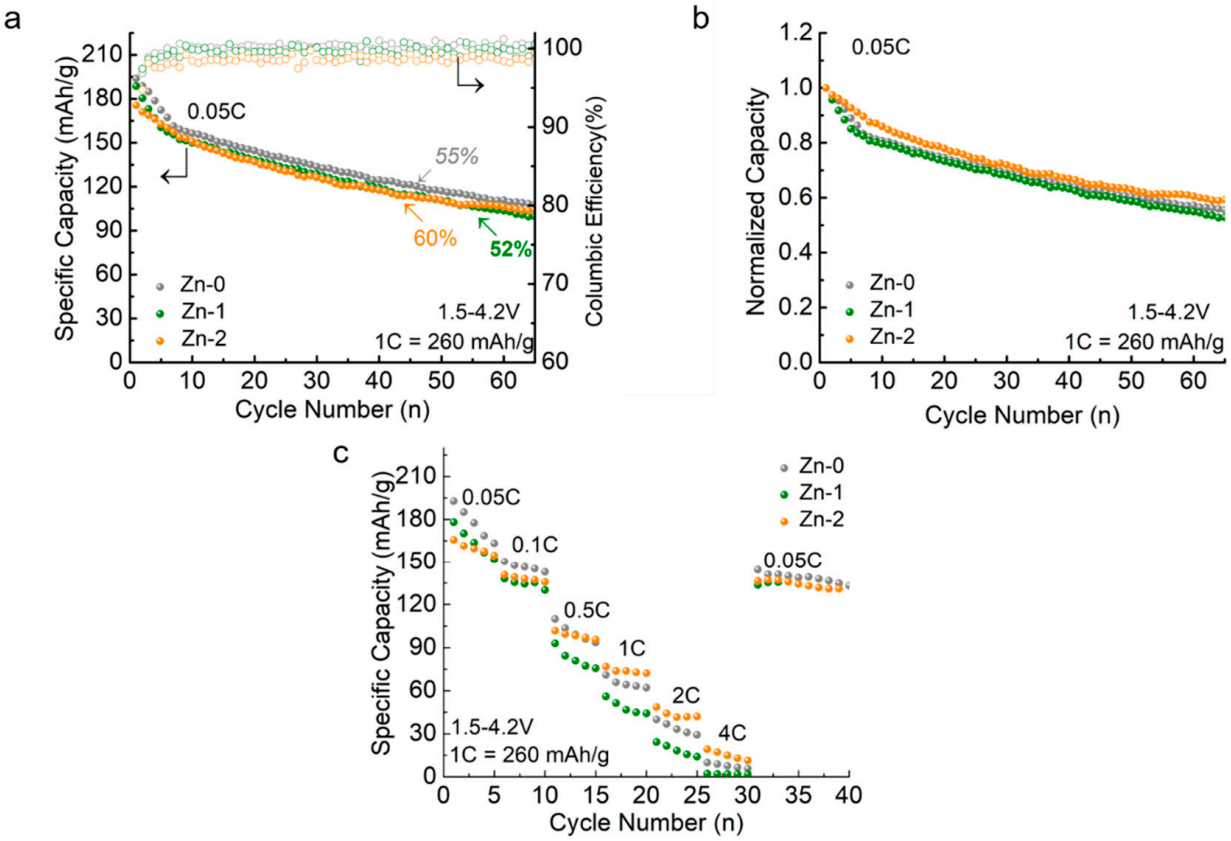

Figure 6. Electrochemical performances of Zn-0, Zn-1 and Zn-2 cathode cycled between 1.5–4.2 V vs. Na/Na^+. (**a**) Cycling stability at 0.05 C (1 C = 260 mA g^{-1}). (**b**) Normalized capacity vs. cycle number. (**c**) Rate performances at different C-rate.

Figure 7 shows the plot for Na content as a function of voltage for Zn-0 and Zn-2 cathode cycled between 1.5–4.2 V vs. Na/Na^+ at 0.05 C. For Zn-0, during the first charge cycle, the final Na content was ~0.22. We assume the theoretical Na content was 0.60 in the beginning of the charge cycle and it was increased to ~0.95 at the end of first discharge cycle. For Zn-2, the Na content after the first charge was around ~0.23 (Na^+ extraction) and increased to ~0.89 at the end of first discharge cycle (Na^+ insertion). Note that the amount of Na^+ ion transport is less for Zn-2 (~0.66) compared to Zn-0 (~0.73) during the first charge-discharge cycle and thus the low specific capacity is observed for the Zn-2 cathode. During the second charge-discharge cycle, Zn-2 (~0.65) shows mostly similar amounts of Na^+ transfer compared to Zn-0 (~0.71) and, consequently, during fifth cycle, Zn-0, and Zn-2 show ~0.65 and ~0.61 respectively. Zn-0 shows decreases in the transport of Na^+ content with the extended cycling compared to Zn-2 and thus a decrease in the specific capacity can be observed. For the Zn-2 cathode, the Na^+ content for the fifth charged cycle was approximately similar amount to the second charged cycle and exhibited higher reversibility when compared to the undoped NFM cathode. The loss of Na^+ in the de/sodiated Zn-0 cathode might be due to several factors such as, structural instability, Fe/Mn migration to Na layer which blocks the diffusion of Na^+ ion and irreversibility of initial phase transition.

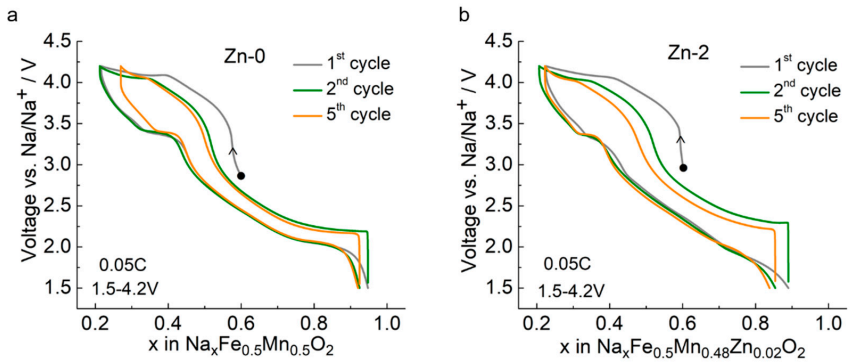

Figure 7. Galvanostatic cycling curve plotted as a function of Na content (x) in (**a**) Zn-0 and (**b**) Zn-2 cathode cycled between 1.5 to 4.2 V vs. Na/Na^+ at 0.05 C. The starting point of the measurement is marked (•).

The galvanostatic charge-discharge curve for Zn-0, Zn-1 and Zn-2 cathodes cycled between 1.5–4.2 V vs. Na/Na^+ at 0.05 C shown in Figure 8. During the first charge (Figure 8a), the plateaus around ~3.5 V corresponds to $Mn^{3+/4+}$, followed by the second plateau at ~4.0 V which is related to oxidation of $Fe^{3+/4+}$. During discharge, the plateaus around ~3.25 V and ~2.0 V corresponds to the reduction of Fe^{4+} and Mn^{4+} respectively. Similar charge discharge profiles are observed in other reports [6,8,19,20,36]. During the first charge, it has been known from the literature [6,14,20] that, above 4.0 V, $Na_{0.66}Fe_{0.5}Mn_{0.5}O_2$ cathode shows phase transition from P2 to OP4 with *P6m2* space group due to stacking faults, where octahedral and prismatic sites are arranged alternatively. We were unable to perform the ex situ XRD due to unavailability of infrastructure. However, we cycled the cathode between 1.5–4.0 V to understand the differences when it is charged above 4.0 V (see Figure 8b). For the Zn-0 cathode, during charging, when cycled above 4.0 V, the charge profile curve obtained indicates the phase transition from P2 to OP4, whereas the charge profile curve for Zn-2 is smoother or more sloped than Zn-0 (see the inset plot in Figure 8a). A similar observation was noticed by Park et al. [8]. To further support the statement, we plotted dq/dV as shown in Figure 8c. We observed comparatively suppressed peak for the Zn-2 cathode sample above 4.0 V, indicating minor phase transition to OP4. This finding can be attributed to the improved structural stability by suppressing the phase transition from P2 to OP4.

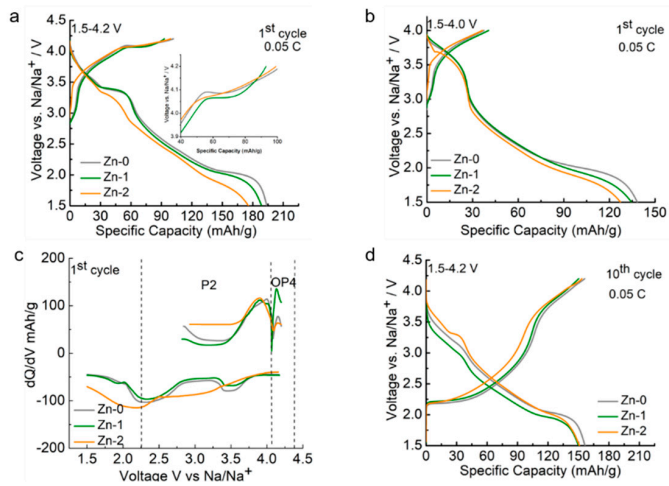

Figure 8. Charge–discharge profile curves for Zn-0, Zn-1 and Zn-2 cathodes cycled between 1.5–4.2 V vs. Na/Na^+ at 0.05 C. (**a**) First cycle, the inset image shows a smooth curve for Zn-2 electrode compared to Zn-0 and Zn-1. (**b**) First cycle in the voltage range of 1.5–4.0 V vs. Na/Na^+. (**c**) dq/dv plot in the voltage range of 1.5–4.2 V for first cycle. (**d**) 10th cycle in the voltage range of 1.5–4.2 V vs. Na/Na^+.

Figure 8d represents the voltage profile curves for the 10th cycle at 0.05 C for Zn-0, Zn-1 and Zn-2 cathode. The iron redox plateau almost vanished for Zn-0 and Zn-1 electrodes, whereas, we can clearly observe the plateau of $Fe^{4+/3+}$ for the Zn-2 electrode. We speculate that there might be migration of Fe^{3+} ions to Na layer and no further redox activity was observed for Fe ions for Zn-0 and Zn-1 cathodes which impedes the Na^{+} ion transport during insertion process [37]. Thus, Zn-2 cathode shows a better electrochemical performance from redox active Fe ions for longer cycles.

The cyclic voltammetry (CV) curves obtained from the assembled Zn-0, Zn-1 and Zn-2 cathode in the coin cell CR2032 vs. lithium metal (detailed fabrication of the coin cell is mentioned in Section 2.3). The coin cell was cycled between 1.5 to 4.2 V vs. Na/Na^{+} at a scan rate of 0.1 mV/s, shown in Figure 9. (Current was normalized based on the active material for the corresponding sample). It has been reported that Mn and Fe both undergo redox reactions over a wide voltage window [9,38]. Zn-0, Zn-1 and Zn-2 peaks correspond to $Mn^{3+/4+}$ at 2.51/1.89 V, 2.59/1.92V, and 2.54/1.84V respectively and $Fe^{3+/4+}$ at 4.19/3.26 V, 4.15/3.26 V and 4.17/3.27 V respectively for the first cycle. These results are complementary to the charge–discharge curves shown in Figure 8. An additional peak (marked with a black arrow in Figure 9c) is observed for Zn-2 sample at around 3.5 V which may be caused by Mn^{3+} induced Jahn–Teller distortion and a similar observation was made by Wang et al. [20]. It can be clearly observed that for the 10th cycle, Zn-2 sample showed a peak at around 3.2 V corresponding to $Fe^{3+/4+}$, but Zn-0 and Zn-1 cathode samples showed very low or no redox. These findings complement the inferences put forth from our electrochemical cycling assessments shown in Figure 8d.

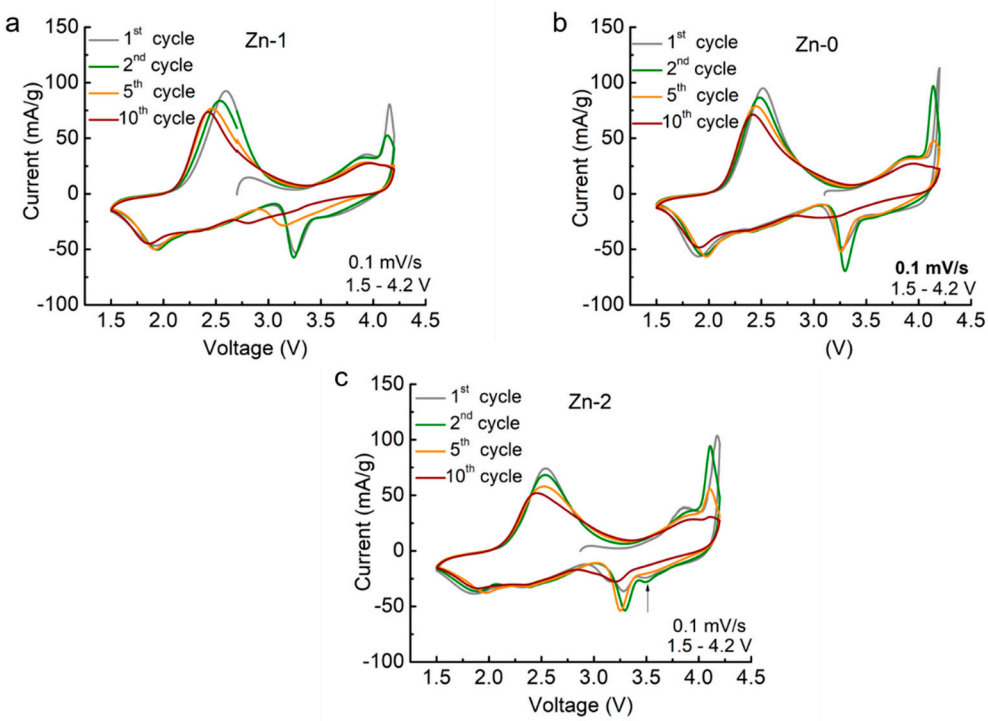

Figure 9. Cyclic voltammetry results of (**a**) Zn-0 (**b**) Zn-1 and (**c**) Zn-2 cathodes in the voltage range of 1.5–4.2 V vs. Na/Na^{+} at a scan rate of 0.1 mV/s.

4. Conclusions

In conclusion, $Na_{0.60}Fe_{0.5}Mn_{0.5}O_2$ cathode material was doped with Zn^{2+} using a sol gel synthesis process followed by detailed structural analysis and electrochemical performance evaluations. Higher quantity of Zn dopant (Zn $\geq$ 2 at.%) resulted in the formation of impurities. Rietveld refinements for Zn-0, Zn-1 and Zn-2 cathodes helped us to understand that Zn-doped NFM cathodes decreased the Na-layer thickness due to

lower bonding energy of Zn-O (ΔHf^{298K} = 284 kJ/mol) in the transition metal layer. For example, calculated Na-layer thickness for Zn-1 was 3.43 Å and Zn-2 was 3.39 Å, showing a decrease by ~2.5–4% compared to the pristine Zn-0. Consequently, the Zn-2 showed minor improvement in the capacity retention of 60% compared to 55% for NFM after 65 cycle, better reversibility and rate performances at higher C-rate. At 1C-rate the Zn-2-doped cathode retained a stable reversible capacity of 72 mAh/g which was ~16% greater than that of NFM (62 mAh/g).This finding can be attributed to an improved structural stability with Zn doping which prevented the phase transition from P2 to OP4 in the first cycle and showed the presence of redox active Fe ions for longer cycles. We believe that this result can further be improved by optimization of cathode materials and particle morphologies.

Supplementary Materials: The following are available online at https://www.mdpi.com/article/10.3390/electrochem2020023/s1. Table S1. Refined crystal sites and atom occupancies of $Na_{0.6}Fe_{0.5}Mn_{0.5}O_2$ (Zn-0) as determined by the Rietveld refinement. Table S2. Refined crystal sites and atom occupancies of $Na_{0.6}Fe_{0.5}Mn_{0.49}$ $Zn_{0.01}O_2$ (Zn-1) as determined by the Rietveld refinement. Table S3. Refined crystal sites and atom occupancies of $Na_{0.6}Fe_{0.5}Mn_{0.42}$ $Zn_{0.02}O_2$ (Zn-2) as determined by the Rietveld refinement.

Author Contributions: D.D.: Formal analysis, Writing—original draft. M.V.R.: Formal analysis, Writing—review & editing, I.B.: Formal analysis, Writing—original draft. All authors have read and agreed to the published version of the manuscript.

Funding: The project was funded by Tennessee Valley Authority (TVA) under the grant # 5315627.

Institutional Review Board Statement: Not applicable.

Informed Consent Statement: Not applicable.

Data Availability Statement: Not applicable.

Acknowledgments: The present work has been carried out with material synthesis and physical characterization at SOLBAT-TTU Energy Research Laboratory, Tennessee Technological University, and electrochemical characterization at Oak Ridge National Laboratory (ORNL), Oak Ridge, Tennessee. Darbar Devendrasinh acknowledges Jagjit Nanda (ORNL) for providing the laboratory facilities for performing the Electrochemical Analysis and Ethan C. Self (ORNL) for helping with the characterization. Indranil Bhattacharya gratefully acknowledges Tennessee Valley Authority (TVA) for providing financial support.

Conflicts of Interest: The authors declare no conflict of interest.

References

1. Han, M.H.; Gonzalo, E.; Singh, G.; Rojo, T. A comprehensive review of sodium layered oxides: Powerful cathodes for Na-ion batteries. *Energy Environ. Sci.* **2015**, *8*, 81–102. [CrossRef]
2. Viciu, L.; Bos, J.W.G.; Zandbergen, H.W.; Huang, Q.; Foo, M.L.; Ishiwata, S.; Ramirez, A.P.; Lee, M.; Ong, N.P.; Cava, R.J. Crystal structure and elementary properties of Nax CoO_2 (x = 0.32, 0.51, 0.6, 0.75, and 0.92) in the three-layer $NaCoO_2$ family. *Phys. Rev. B Condens. Matter Mater. Phys.* **2006**, *73*, 174104. [CrossRef]
3. Billaud, J.; Clément, R.J.; Armstrong, A.R.; Canales-Vázquez, J.; Rozier, P.; Grey, C.P.; Bruce, P.G. β-$NaMnO_2$: A High-Performance Cathode for Sodium-Ion Batteries. *J. Am. Chem. Soc.* **2014**, *136*, 17243–17248. [CrossRef] [PubMed]
4. Zhao, J.; Zhao, L.; Dimov, N.; Okada, S.; Nishida, T. Electrochemical and Thermal Properties of α-$NaFeO_2$ Cathode for Na-Ion Batteries. *J. Electrochem. Soc.* **2013**, *160*, A3077–A3081. [CrossRef]
5. Kim, D.; Lee, E.; Slater, M.; Lu, W.; Rood, S.; Johnson, C.S. Layered $Na[Ni_{1/3}Fe_{1/3}Mn_{1/3}]O_2$ cathodes for Na-ion battery application. *Electrochem. Commun.* **2012**, *18*, 66–69. [CrossRef]
6. Yabuuchi, N.; Kajiyama, M.; Iwatate, J.; Nishikawa, H.; Hitomi, S.; Okuyama, R.; Usui, R.; Yamada, Y.; Komaba, S. P2-type $Nax[Fe_{1/2}Mn_{1/2}]O_2$ made from earth-abundant elements for rechargeable Na batteries. *Nat. Mater.* **2012**, *11*, 512–517. [CrossRef] [PubMed]
7. Yoshida, H.; Yabuuchi, N.; Komaba, S. $NaFe_{0.5}Co_{0.5}O_2$ as high energy and power positive electrode for Na-ion batteries. *Electrochem. Commun.* **2013**, *34*, 60–63. [CrossRef]
8. Park, J.; Park, G.; Kwak, H.H.; Hong, S.-T.; Lee, J. Enhanced Rate Capability and Cycle Performance of Titanium-Substituted P2-Type $Na_{0.67}Fe_{0.5}Mn_{0.5}O_2$ as a Cathode for Sodium-Ion Batteries. *ACS Omega* **2018**, *3*, 361–368. [CrossRef]
9. Kalluri, S.; Seng, K.H.; Pang, W.K.; Guo, Z.; Chen, Z.; Liu, H.-K.; Dou, S.X. Electrospun P2-type $Na_{2/3}(Fe_{1/2}Mn_{1/2})O_2$ Hierarchical Nanofibers as Cathode Material for Sodium-Ion Batteries. *ACS Appl. Mater. Interfaces* **2014**, *6*, 8953–8958. [CrossRef] [PubMed]

10. Xu, J.; Chou, S.-L.; Wang, J.-L.; Liu, H.-K.; Dou, S.-X. Layered P2-$Na_{0.66}Fe_{0.5}Mn_{0.5}O_2$ Cathode Material for Rechargeable Sodium-Ion Batteries. *ChemElectroChem* **2014**, *1*, 371–374. [CrossRef]
11. Han, M.H.; Gonzalo, E.; Sharma, N.; López del Amo, J.M.; Armand, M.; Avdeev, M.; Saiz Garitaonandia, J.J.; Rojo, T. High-Performance P2-Phase $Na_{2/3}Mn_{0.8}Fe_{0.1}Ti_{0.1}O_2$ Cathode Material for Ambient-Temperature Sodium-Ion Batteries. *Chem. Mater.* **2016**, *28*, 106–116. [CrossRef]
12. Kalapsazova, M.; Ortiz, G.F.; Tirado, J.L.; Dolotko, O.; Zhecheva, E.; Nihtianova, D.; Mihaylov, L.; Stoyanova, R. *P* 3-Type Layered Sodium-Deficient Nickel-Manganese Oxides: A Flexible Structural Matrix for Reversible Sodium and Lithium Intercalation. *Chempluschem* **2015**, *80*, 1642–1656. [CrossRef]
13. Guo, S.; Liu, P.; Yu, H.; Zhu, Y.; Chen, M.; Ishida, M.; Zhou, H. A Layered P2- and O3-Type Composite as a High-Energy Cathode for Rechargeable Sodium-Ion Batteries. *Angew. Chem. Int. Ed.* **2015**, *54*, 5894–5899. [CrossRef] [PubMed]
14. Mortemard de Boisse, B.; Carlier, D.; Guignard, M.; Delmas, C. Structural and Electrochemical Characterizations of P2 and New O3-$Na_x Mn_{1-y} Fe_y O_2$ Phases Prepared by Auto-Combustion Synthesis for Na-Ion Batteries. *J. Electrochem. Soc.* **2013**, *160*, A569–A574. [CrossRef]
15. Zhao, J.; Xu, J.; Lee, D.H.; Dimov, N.; Meng, Y.S.; Okada, S. Electrochemical and thermal properties of P2-type $Na_{2/3}Fe_{1/3}Mn_{2/3}O_2$ for Na-ion batteries. *J. Power Sources* **2014**, *264*, 235–239. [CrossRef]
16. Carlier, D.; Cheng, J.H.; Berthelot, R.; Guignard, M.; Yoncheva, M.; Stoyanova, R.; Hwang, B.J.; Delmas, C. The P2-$Na_{2/3}Co_{2/3}Mn_{1/3}O_2$ phase: Structure, physical properties and electrochemical behavior as positive electrode in sodium battery. *J. Chem. Soc. Dalt. Trans.* **2011**, *40*, 9306–9312. [CrossRef]
17. Shanmugam, R.; Lai, W. $Na_{2/3}Ni_{1/3}Ti_{2/3}O_2$: "Bi-Functional" Electrode Materials for Na-Ion Batteries. *ECS Electrochem. Lett.* **2014**, *3*, A23–A25. [CrossRef]
18. Mohanty, D.; Dahlberg, K.; King, D.M.; David, L.A.; Sefat, A.S.; Wood, D.L.; Daniel, C.; Dhar, S.; Mahajan, V.; Lee, M.; et al. Modification of Ni-Rich FCG NMC and NCA Cathodes by Atomic Layer Deposition: Preventing Surface Phase Transitions for High-Voltage Lithium-Ion Batteries. *Sci. Rep.* **2016**, *6*, 1–16. [CrossRef] [PubMed]
19. Talaie, E.; Duffort, V.; Smith, H.L.; Fultz, B.; Nazar, L.F. Structure of the high voltage phase of layered P2-$Na_{2/3-z}[Mn_{1/2}Fe_{1/2}]O_2$ and the positive effect of Ni substitution on its stability. *Energy Environ. Sci.* **2015**, *8*, 2512–2523. [CrossRef]
20. Wang, H.; Gao, R.; Li, Z.; Sun, L.; Hu, Z.; Liu, X. Different Effects of Al Substitution for Mn or Fe on the Structure and Electrochemical Properties of $Na_{0.67}Mn_{0.5}Fe_{0.5}O_2$ as a Sodium Ion Battery Cathode Material. *Inorg. Chem.* **2018**, *57*, 5249–5257. [CrossRef] [PubMed]
21. Li, Z.-Y.; Gao, R.; Sun, L.; Hu, Z.; Liu, X. Zr-doped P2-Na0.75Mn0.55Ni0.25Co0.05Fe0.10Zr0.05O2 as high-rate performance cathode material for sodium ion batteries. *Electrochim. Acta* **2017**, *223*, 92–99. [CrossRef]
22. Tiwari, B.; Bhattacharya, I. Layered P2- type novel $Na_{0.7}Ni_{0.3}Mn_{0.59}Co_{0.1}Cu_{0.01}O_2$ cathode material for high-capacity & stable rechargeable sodium ion battery. *Electrochim. Acta* **2018**, *270*, 363–368. [CrossRef]
23. Darbar, D.; Muralidharan, N.; Hermann, R.P.; Nanda, J.; Bhattacharya, I. Evaluation of Electrochemical Performance and Redox Activity of Fe in Ti doped Layered P2-$Na_{0.67}Mn_{0.5}Fe_{0.5}O_2$ Cathode for Sodium Ion Batteries. *Electrochim. Acta* **2021**, *380*, 138156. [CrossRef]
24. Mao, Q.; Zhang, C.; Yang, W.; Yang, J.; Sun, L.; Hao, Y.; Liu, X. Mitigating the voltage fading and lattice cell variations of O_3-$NaNi_{0.2}Fe_{0.35}Mn_{0.45}O_2$ for high performance Na-ion battery cathode by Zn doping. *J. Alloy. Compd.* **2019**, *794*, 509–517. [CrossRef]
25. Aguesse, F.; Lopez del Amo, J.M.; Otaegui, L.; Goikolea, E.; Rojo, T.; Singh, G. Structural and electrochemical analysis of Zn doped Na3Ni2SbO6 cathode for Na-ion battery. *J. Power Sources* **2016**, *336*, 186–195. [CrossRef]
26. Wang, P.F.; Guo, Y.J.; Duan, H.; Zuo, T.T.; Hu, E.; Attenkofer, K.; Li, H.; Zhao, X.S.; Yin, Y.X.; Yu, X.; et al. Honeycomb-Ordered $Na_3Ni_{1.5}M_{0.5}Bi_{O6}$ (M = Ni, Cu, Mg, Zn) as High-Voltage Layered Cathodes for Sodium-Ion Batteries. *ACS Energy Lett.* **2017**, *2*, 2715–2722. [CrossRef]
27. Wang, K.; Yan, P.; Wang, Z.; Fu, J.; Zhang, Z.; Ke, X.; Sui, M. Advancing layered cathode material's cycling stability from uniform doping to non-uniform doping. *J. Mater. Chem. A* **2020**, *8*, 16690–16697. [CrossRef]
28. Xu, H.; Zong, J.; Liu, X.J. P2-type $Na_{0.67}Mn_{0.6}Fe_{0.4-x-y}Zn_xNi_yO_2$ cathode material with high-capacity for sodium-ion battery. *Ionics* **2018**, *24*, 1939–1946. [CrossRef]
29. Wu, X.; Xu, G.L.; Zhong, G.; Gong, Z.; McDonald, M.J.; Zheng, S.; Fu, R.; Chen, Z.; Amine, K.; Yang, Y. Insights into the Effects of Zinc Doping on Structural Phase Transition of P2-Type Sodium Nickel Manganese Oxide Cathodes for High-Energy Sodium Ion Batteries. *ACS Appl. Mater. Interfaces* **2016**, *8*, 22227–22237. [CrossRef]
30. Hellenbrandt, M. The Inorganic Crystal Structure Database (ICSD)—Present and Future. *Crystallogr. Rev.* **2004**, *10*, 17–22. [CrossRef]
31. Delmas, C.; Braconnier, J.-J.; Fouassier, C.; Hagenmuller, P. Electrochemical intercalation of sodium in NaxCoO2 bronzes. *Solid State Ion.* **1981**, *3–4*, 165–169. [CrossRef]
32. Shannon, R.D. Revised effective ionic radii and systematic studies of interatomic distances in halides and chalcogenides. *Acta Crystallogr. Sect. A* **1976**, *32*, 751–767. [CrossRef]
33. Li, Z.-Y.; Wang, H.; Yang, W.; Yang, J.; Zheng, L.; Chen, D.; Sun, K.; Han, S.; Liu, X. Modulating the Electrochemical Performances of Layered Cathode Materials for Sodium Ion Batteries through Tuning Coulombic Repulsion between Negatively Charged TMO_2 Slabs. *ACS Appl. Mater. Interfaces* **2018**, *10*, 1707–1718. [CrossRef] [PubMed]

34. Momma, K.; Izumi, F. IUCr *VESTA 3* for three-dimensional visualization of crystal, volumetric and morphology data. *J. Appl. Crystallogr.* **2011**, *44*, 1272–1276. [CrossRef]
35. Speight, D.J.G. *Lange's Handbook of Chemistry*, 17th ed.; McGraw-Hill Education: New York, NY, USA, 2017; ISBN 9781259586095.
36. Mortemard de Boisse, B.; Carlier, D.; Guignard, M.; Bourgeois, L.; Delmas, C. P2-$Na_xMn_{1/2}Fe_{1/2}O_2$ Phase Used as Positive Electrode in Na Batteries: Structural Changes Induced by the Electrochemical (De)intercalation Process. *Inorg. Chem.* **2014**, *53*, 11197–11205. [CrossRef]
37. Li, X.; Wang, Y.; Wu, D.; Liu, L.; Bo, S.H.; Ceder, G. Jahn-Teller assisted Na diffusion for high performance Na ion batteries. *Chem. Mater.* **2016**, *28*, 6575–6583. [CrossRef]
38. Yuan, D.; Hu, X.; Qian, J.; Pei, F.; Wu, F.; Mao, R.; Ai, X.; Yang, H.; Cao, Y. P2-type $Na_{0.67}Mn_{0.65}Fe_{0.2}Ni_{0.15}O_2$ Cathode Material with High-capacity for Sodium-ion Battery. *Electrochim. Acta* **2014**, *116*, 300–305. [CrossRef]